Constructing Virtual Mines for Navigation

Frédéric Labrosse, Jean-Yves Hervé, and Paul Cohen

Groupe de Recherche
en
Perception et Robotique

École Polytechnique de Montréal
GRPR - DGEGI
P.O. Box 6079, Station Centre-ville
Montréal (Québec) CANADA H3C 3A7
tel: (514)340-5783, fax: (514)340-5802

e-mail: `[labrosse,jyh,cohen]@ai.polymtl.ca`

To appear in: Proceedings of the IEEE Conference on Systems, Man, and Cybernetics, Orlando, Floride, octobre 1997

Constructing Virtual Mines for Navigation

Frédéric Labrosse, Jean-Yves Hervé, and Paul Cohen

Groupe de Recherche en Perception et Robotique
Département de Génie Électrique et de Génie Informatique
École Polytechnique, Montréal, Québec, Canada

[labrosse,jyh,cohen]@ai.polymtl.ca

Abstract

This article presents an underground mine model created to study such tasks as autonomous navigation, obstacle avoidance, exploration and surveying, or place recognition. We first describe the generic object model upon which the mine model is based, and then describe the mine model itself. To study the aforementioned problems, we have developed a software package that uses a mine representation (an instance of the model) as input and generates virtual mines used as simulation environments. We then describe the complementary problem of how to construct mine representations from surveying data.

1 Introduction

An important part of the mining automation process is the development of autonomous navigation and related tasks such as obstacle avoidance, automated surveying, trajectory planning, or place recognition. Some of these tasks need a representation of the environment (an underground mine in our case), some produce such a representation, and others only need local "views" of the environment. "Views" can consist of photometric or range images.

In the representation of mines, we need to distinguish between such components as drifts[1], stopes[2], and intersections because the tasks to be performed and the ways navigation is done are different in these areas. We want a multi-scale representation in order to represent, *e.g.*, drifts in their whole and as succession of parts to clearly identify local properties such as curvature. There are other attributes than geometry to represent: surface roughness and rock type can help to predict noise in range images; lighting can be used, *e.g.*, to plan paths that are illuminated everywhere or, in an other context, to reason about where to place lights in order to maximize illuminated areas; obstacles, when known, can be included in the mine representation.

Existing mine models are essentially of two kinds. One is the so-called block model, which represents volumes by their decomposition into small blocks whose shape and dimension can be regular or not. This type of model is useful to represent volumetric properties such as ore bodies [6, 11, 10]. Models of the second type are CAD models. They represent volume boundaries with triangulated surfaces [10, 5, 1, 14, 12].

Neither CAD models nor block models are suitable for navigation tasks and we thus have developed our own underground mine model, which is based on a generic object model [9].

The representation of a mine following this model can be used as input to a software package we have developed to produce a virtual mine environment that can be used to study navigational problems. Such representations are built from surveying data that can be of two types: the first is produced by traditional (manual) surveying while the second is the result of automated surveying.

Section 2 briefly introduces the generic object model, while Section 3 describes the underground mine model. Section 4 explains how we construct mine representations from surveying data.

2 The Generic Object Model

In order to represent the multitude of objects involved in robotics tasks, we have developed a GeNeric Object ModEl (GNOME). In GNOME, an object is described by a set of *attributes* (*e.g.* geometry, color, density, or temperature). This model is independent of the task to perform with the represented object and of the agent performing the task. The representation (an instance of GNOME) of a given object, however, depends on the task and the agent.

In the next sections, we will describe the three model's parts, the *structure*, the *quantification*, and the *inter-attribute relations* graph. A more complete description as well as a formalization of GNOME can be found in [9].

2.1 The Object's *Structure*

Each attribute takes its values in a particular space, *e.g.* an RGB space for color. The attribute's values can be grouped in this space to construct objects, which we will call *attribute-objects*. These can be, for instance, raw forms like cubes or spheres in the geometric at-

This work was supported by the industrial partnership program of the Natural Sciences and Engineering Research Council of Canada (NSERC-Noranda chair in mining automation).

[1]A Drift is a horizontal underground opening.

[2]A stope is an underground excavation that is made by removing ore from the surrounding rock. By extension, all large openings are named stopes.

tribute. Higher level attribute-objects, like chairs or tables, are decomposed into more basic attribute-objects. This decomposition can be functional, can be based on geometry (or any other attribute), can follow a notion of scale or abstraction, or can be a combination of such criteria. Thus, there is a hierarchy in the set of all the attribute-objects. This hierarchy is represented by a *decomposition tree*.

Moreover, relations exist between the attribute-objects, which are the nodes of the decomposition tree. These relations can be connection, relative pose, ordinal relations, *etc.* They are represented by a graph whose nodes are the decomposition tree's nodes and whose arcs indicate relations between attribute-objects.

There is a tree and graph for each attribute, and the set of all trees and graphs for all attributes constitutes the represented object's *structure*.

2.2 The Object's *Quantification*

The attribute-objects can be quantified to specify attribute values. For example, the quantification specifies the side of a "geometric" cube, a color's value in RGB space, or the values of a surface's equation parameters.

The relations between attribute-objects can be quantified as well. To do this, we transform the graph representing the relations into a *labeled graph*, *i.e.* a graph whose arcs have labels associated to them indicating which relations they represent as well as their quantification.

The set of all quantifications of attribute-objects and relations for all attributes is the quantification of the represented object.

2.3 The Graph of *Inter-attribute Relations*

Up to now, the attributes have been represented independently. In fact, they are usually not independent, and we must represent the inter-attribute relations. These relations involve attribute-objects from different attributes and their quantifications. Thus, the inter-attribute relations constitute a graph whose nodes are attribute-objects and quantifications. In fact, the graph is labeled since the inter-attribute relations can be quantified.

One particular inter-attribute relation is *correspondence*, which allows the qualitative association of attribute-objects from different attributes. For example, a correspondence can state that a particular geometric part is red while another part has a green gradation or that, in an infra-red image, red corresponds to high temperatures while blue to low temperatures.

3 GNOMine: The Mine Model

As mentioned in Section 1, we have included the following attributes in the mine model (GNOMine): geometry, surface roughness, rock type, lighting, and obstacles. From the point of view of navigation, geometry is the most important attribute. The other attributes, however, allow us to describe the environment more completely. Moreover, additional attributes can be included in the model.

We first describe the geometrical attribute, in particular the decomposition that leads to the different geometrical parts of the mine; we then describe the other attributes. A complete description of the mine model can be found in [8].

3.1 The Mine's Geometry

3.1.1 The Decomposition

In an underground mine, there are essentially two navigational modes: drift following and navigation in large spaces (intersections and stopes). This has guided our decision to decompose the mine into drifts, intersections, and stopes.

In order to represent drifts with a sufficient level of detail and complexity, they are decomposed into drift sections. The model's purpose being for navigation, sections are represented as clothoidal ribbons with a constant width and height[3]. Moreover, we impose that the curve formed by the axis of the sections composing a drift be continuous in position, orientation, and curvature. This constraint is to ensure that a drift can be followed by a vehicle[4]. Each drift section is quantified by its width, height, length, and all necessary parameters to specify its axis, *i.e.* initial curvature and rate of variation of curvature.

The 2D space composing an intersection or stope is represented by its boundaries. These are, at a first level, composed of walls, *i.e.* the vertical parts joining the ends of (adjacent) drifts. The quantification of an intersection consists of the translations and rotations between its various exits (to which reference systems are attached, Figure 2). At a second level, each wall is split into wall sections of low curvature[5]. Wall sections are represented as 3D cubic curves; the first two coordinates represent the wall's horizontal shape and the last coordinate represent the wall's height. Wall sections are quantified by the parameters of the cubic curve.

The mine's decomposition introduces other geometrical parts such as floors and ceilings. The complete generic decomposition is shown in Figure 1.

---

[3]Clothoids are useful to represent drifts as they can be followed by vehicles [4] and are widely used in autonomous navigation [3, 7]. A clothoid is a curve whose curvature varies linearly with arc length:

$$\kappa(s) = \kappa_0 + ks,$$

where $\kappa(s)$ is the curvature, s is the arc length, κ_0 is the initial curvature, and k is the rate of variation of curvature.

[4]In case of a drift that cannot satisfy this constraint, a geometrical part (topologically analogous to an intersection) is introduced in the decomposition.

[5]Decomposition takes place where the wall presents an angle, *i.e.* places of high curvature.

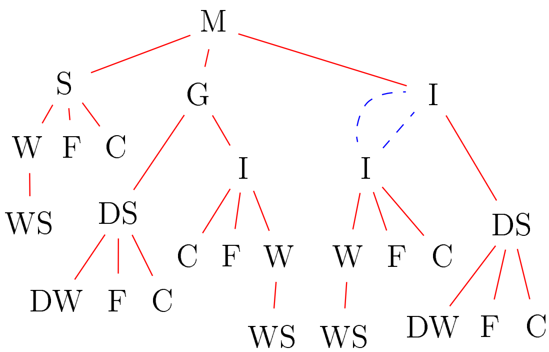

Figure 1: The generic decomposition tree for geometry. Dashed lines indicate possible recursion. (One level of recursion is shown.) C: ceiling, F: floor, DS: drift section, DW: drift wall, I: intersection, M: mine, W: wall, WS: wall section.

3.1.2 The Relations

Two relations exist between the geometrical parts: the *connection* and the *attachment*. The former is qualitative and involves drifts, intersections, and stopes. It is useful to establish a (qualitative) road-book. The latter specifies how drift sections are attached to intersections and stopes. By "how" we mean by which of their reference systems. Each of the concerned attribute-objects has thus several coordinate systems, one for each exit, oriented such that the z axis is ingoing. Figure 2 shows some objects with their coordinate systems. The attachment is quantified by the reference systems indexes of the two attached objects.

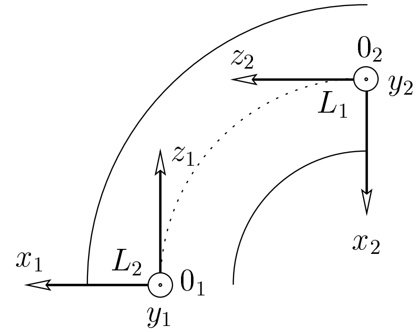

(a) For a drift section

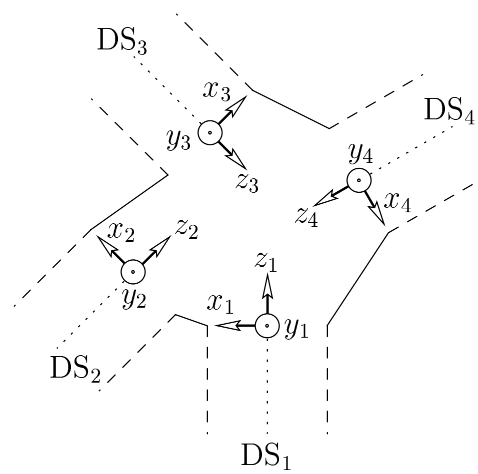

(b) For an intersection

Figure 2: Coordinate systems

3.2 The Other Attributes of the Mine

Surface roughness is represented by three parameters: a fractal dimension, a bump density, and an average bump deviation. Roughness attribute-objects are thus quantified by three real numbers.

Rock types are represented by a classical geological taxonomy, which is similar to the decomposition tree of GNOME. Nodes can be quantified by the grade of rock (or ore).

Obstacles are geometrical objects (not included in the geometric attribute) positioned in the mine. We have so far retained two obstacle types: a parallelepiped to represent boulders and a cone to represent stone heaps.

There are currently three basic lighting types. The first is a *point light* to represent light bulbs at strategic places (such as intersections or dangerous places) in the mine. The second is a *directional light* to represent ambient lighting provided by a large set of lamps on the ceilings of stopes where regular activity occurs (*e.g.* workshops or staff stopes). The third is a *spotlight* to represent vehicle beams. If one wishes to include vehicles in the mine model, spotlights can be combined to give *vehicle lighting*, a higher level lighting attribute-object carried by a vehicle.

These particular models of obstacles and light sources are sufficient to cover a large number of mining environments. Other models, however, could be added, or substituted, to these without modifying the general structure of GNOMine.

3.3 Inter-attribute Relations

Several inter-attribute relations are required in GNOMine. There are indeed correspondences between geometry and surface roughness or rock type (all surfaces have roughness values and rock types), between geometry and lighting (to place directional lights in stopes), and between obstacles and surface roughness or rock type. There are also quantitative relations to place obstacles and lights in the geometry. For example, one such relation positions a moving vehicle alternately in drift sections, intersections, or stopes. The quantification of this relation is thus time-varying and involves a process of destruction-creation of associations between the vehicle and geometrical parts.

Based on this mine model, we have developed a software package that builds a virtual mine from its representation (an instance of GNOMine). Figure 3 shows two views, one with only surface roughness (top) and another with all attributes (bottom).

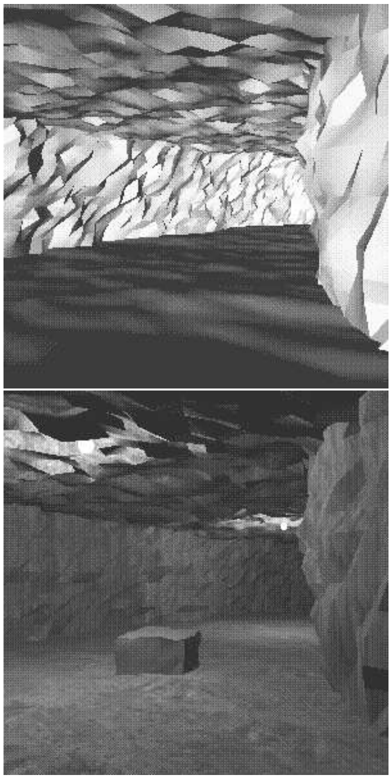

Figure 3: Some views of a virtual mine with different attributes

4 Constructing Representations

We explain here how to construct geometric mine representations based on GNOMine using real surveying data as input (Section 4.1). We first pre-segment each drift into drift sections and each intersection wall into wall sections to establish the number of sections and raw estimates of their parameters (Section 4.3). We then proceed to an optimization phase to determine the "best" parameters (Section 4.4). Section 4.5 shows some results of reconstruction.

4.1 Surveying Data

The mining industry has accumulated vast amount of surveying data. These data consist of sparse measurements, made manually by human surveyors, of important features in the mine; the measurements are reported in a global reference system. More details can be found in [15] on the techniques for mine surveying.

Here, we prefer to use surveying data gathered during the exploration of the mine by an autonomous vehicle. This vehicle initially possesses a topological description, under the form of a graph, of the mine and have to drive through all the mine. It uses range profiles as sensory data to detect events such as arrival at intersection and localize itself in the graph. During the mine traversal, the vehicle acquires lateral and top range profiles that are used to produce data representing ground plane and height measurements of walls of drifts, intersections, and stopes. These measurements consist of 3D points in a global coordinate system. The problems of robot navigation and localization in a mine environment is addressed in [2].

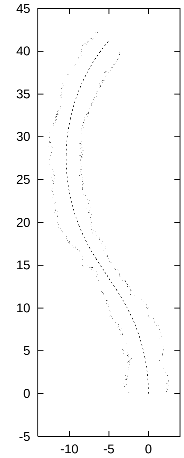

Figure 4: Artificial surveying data for a drift. The axis of the drift is also shown.

To test our reconstruction method, we artificially generate such data by applying a random fractal shape [13] and noise to ideal drifts and intersections, then randomly choose points as measurements. Figure 4 shows such artificial surveying data for a drift.

4.2 Parameters to Calculate

In order to describe the succession of continuous clothoidal drift sections, we use the following vector of parameters:

$$\mathbf{p} = (x_0, y_0, \tau_0, \kappa_0, k_1, w_1, h_1, s_{02}, k_2, \cdots, w_n, h_n), \quad (1)$$

where (x_0, y_0) is the position of the drift's starting point, and τ_0 and κ_0 are respectively the orientation, and curvature at this point. Similarly, s_{0i} is the (cumulated) arc length at the starting point of the ith drift section[6], while k_i, w_i, and h_i are respectively the rate of variation of curvature, width, and height of this drift section. Finally, n is the number of sections that compose the drift. We want to determine $\mathbf{p}$ such that

$$\begin{aligned} D(\mathbf{p}) &= \sum_k d^2(\mathbf{M}_{L_k}, \mathbf{A}_L(\mathbf{p})) \\ &+ \sum_k d^2(\mathbf{M}_{R_k}, \mathbf{A}_R(\mathbf{p})), \end{aligned} \quad (2)$$

is minimized, where $d(\cdot,\cdot)$ is the Euclidean distance between two points and $\mathbf{A}_L(\mathbf{p})$ [resp. $\mathbf{A}_R(\mathbf{p})$] is the axis point of the parameter $\mathbf{p}$ drift nearest to the kth left measure $\mathbf{M}_{L_k}$ [resp. right measure $\mathbf{M}_{R_k}$].

For a wall, the parameter vector is:

$$\mathbf{p} = (\mathbf{e}_{01}, \mathbf{t}_{01}, \mathbf{t}_{11}, \mathbf{e}_{11}, \mathbf{t}_{02}, \mathbf{t}_{12}, \cdots, \mathbf{e}_{1n}), \quad (3)$$

where $\mathbf{e}_{0i}$, $\mathbf{t}_{0i}$, $\mathbf{t}_{1i}$, and $\mathbf{e}_{1i}$ are the position and tangent direction at either endpoint of the ith cubic curve[7].

[6] s_{01} is always zero and is therefore not included.

[7] Due to continuity in position of wall sections composing a wall, we have $\mathbf{e}_{1i} \equiv \mathbf{e}_{0i+1}$.

The goal is to minimize

$$D(\mathbf{p}) = \sum_k d^2(\mathbf{c}(\mathbf{p}), \mathbf{M}_k), \tag{4}$$

where $\mathbf{c}(\mathbf{p})$ is the point of the parameter $\mathbf{p}$ curve nearest to the kth measure $\mathbf{M}_k$.

4.3 Pre-segmentation

As previously mentioned, the first step of reconstruction is to pre-segment measurements of drifts or intersection walls to (1) establish the number of sections and (2) calculate a raw estimate of their parameters. For the drift case, the segmentation is based upon the uniformity of (1) the rate of variation of curvature k of the axis, (2) the width w of the drift, and (3) the height h of the drift. In the case of intersection walls, the segmentation is based upon a single criterion: low value of the wall curvature.

4.4 Optimization

The parameters determined in Section 4.3 are used as starting values for a global minimization (for each drift and wall) of (2) and (4). Due to the high dimensionality of the minimization spaces as well as the high non-convexity and instability of the functions to minimize (especially in the case of the drifts due to the imposed continuity of curvature), we use a simulated annealing procedure. The selected implementation was previously known as Very Fast Simulated Re-annealing and is now distributed as Adaptive Simulated Annealing[8].

4.5 Results

Figure 5 illustrates the reconstruction of a drift, in the ground plane and in vertical cross-section. Likewise, Figure 6 shows the reconstruction of intersection walls (seen in ground plane).

To evaluate these results, we must compare a given reconstruction to the ideal drift or intersection that provided the surveying data (Section 4.1). However, the fractal shape and noise introduced are such that the survey data is biased with respect to the initial structure. Thus, to do the comparison, we generate several sets of surveying data by applying different fractal shapes and noises to the same initial structure. We can then compare the ideal parameters and the average reconstruction ones. Table 1 shows the average result of ten reconstruction trials for a three-section drift. Two of the trials led to a segmentation into four sections: in one case, because the surveying data presents two very different heights in the second section; in the other case, because the median axis presents a straight portion at its end (due to filtering). From Table 1, we can see that the greatest deviation is at the drift starting point, due to a quite low density of measurements (see later).

[8]This implementation as been found at the web address `http://www.ingber.com/` and is the result of the work of Lester Ingber and other contributors.

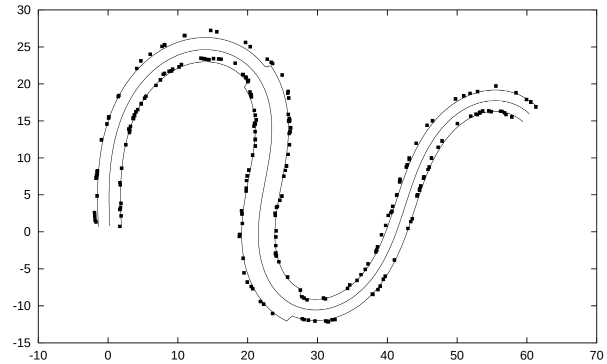

(a) The drift's walls

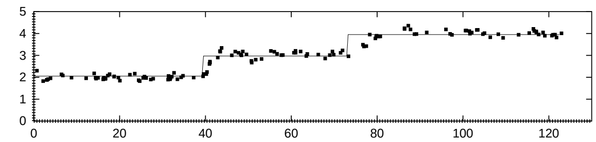

(b) The drift's height

Figure 5: Reconstruction of a drift. Dots represent measurements.

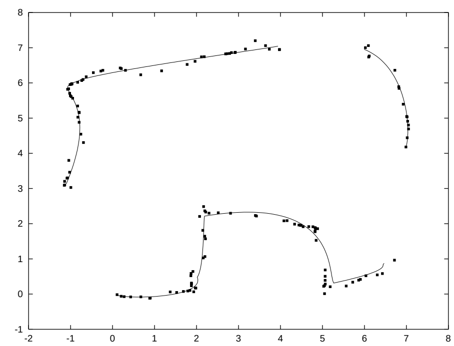

Figure 6: The reconstruction of an intersection

The effect of measurement density is also interesting to analyze. The results show that the reconstruction quality diminishes somewhat as the measurement density decreases. In the case of stopes, this is due to two causes. First, the pre-segmentation produces generally more sections when based upon the curvature (because the median axis orientation becomes less continuous as the measurement density lowers) but fewer when based upon width and height (because these functions become sparser, thereby eliminating constant regions). Second, the minimization is less constrained, thus more difficult, especially near the drift's starting point. The starting point of sections are also positioned less accurately. For the case of walls, angles are generally not detected, leading to a small number of sections, but the final distance between reconstructed walls and measurements, while increasing (Table 2), remains acceptable (Figure 7).

5 Conclusion

We presented an underground mine model (GNOMine) for the study of navigational tasks, such as autonomous

Table 1: The average parameters of ten drift reconstructions and the parameters of the perfect structure used to produce measurements (see text)

	Struct.	Ave.		Struct.	Ave.
L	125.00	124.16	s_{02}	40.00	40.17
x_0	0.00	0.32	k_2	0.00750	0.00749
y_0	0.00	0.60	l_2	5.00	4.90
τ_0	1.57	1.63	h_2	3.00	3.01
κ_0	0.0000	-0.0056	s_{03}	75.00	75.17
k_1	-0.0030	-0.0028	k_3	-0.0060	-0.0060
l_1	3.50	3.58	l_3	3.00	3.03
h_1	2.00	2.02	h_3	4.00	3.94

Table 2: Wall reconstruction: average distance and number of wall sections for several measure densities

Density	20	10	5	2	1
Distance (cm)	19.2	18.0	19.5	45.1	54.4
Sections	7	7	6	3	2

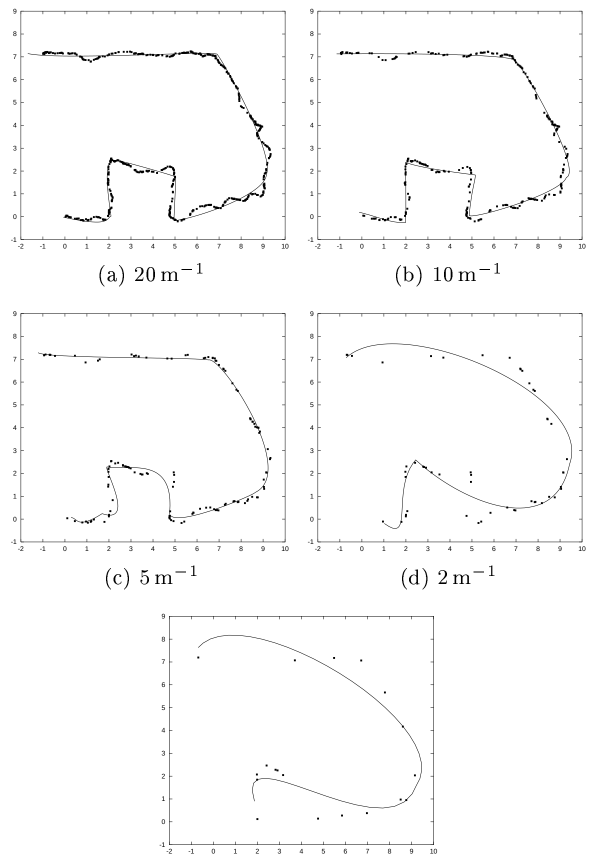
(a) $20\,\mathrm{m}^{-1}$ (b) $10\,\mathrm{m}^{-1}$ (c) $5\,\mathrm{m}^{-1}$ (d) $2\,\mathrm{m}^{-1}$ (e) $1\,\mathrm{m}^{-1}$

Figure 7: A wall reconstructed with several measure densities

navigation, obstacle avoidance, automated surveying, and intersection recognition. We also described the generic object model GNOME from which the mine model was developed. We then describe the construction of geometric representations based upon this model. Some results have been presented.

It remains to reconstruct the other attributes and to automatically build the inter-attribute relations graph. For example, the surface roughness could be reconstructed by statistically analyzing very dense measurements. Obstacles have to be detected during traversals of the mine by vehicles and then positioned in the mine representation. Lights are also positioned in the representation based on information provided by the maintenance staff.

References

[1] P. Campbell and B. Smith. An integrated mine planning system for geology, surveying, and engineering. In *Proc. Canadian Conf. on Comp. Appl. in the Mineral Industry*, pages 115–126, Vancouver, BC, Canada, Sept. 1991.

[2] P. Debanné, J.-Y. Hervé, and P. Cohen. Global self-localization of a robot in underground mines. 1997. In these proceedings.

[3] E. D. Dickmanns, B. D. Mysliwetz, and T. Christians. An integrated spatio-temporal approach to automatic visual guidance of autonomous vehicles. *IEEE TSMC*, 20(6):1273–1284, 1990.

[4] S. Fleury, P. Souères, J.-P. Laumond, and R. Chatila. Primitives for smoothing mobile robot trajectories. *IEEE TRA*, 11(3):441–448, 1995.

[5] S. Henley and A. Wheeler. The use of solid modelling in underground mine design. In *Proc. Canadian Conf. on Comp. Appl. in the Mineral Industry*, pages 359–364, Québec, QC, Canada, Mar. 1988.

[6] J. A. Horst and T.-M. Tsai. Building and maintaining computer representations of two-dimensional mine maps. In *Proceedings of the International Symposium on Mine Mechanization and Automation*, volume 2, pages 22–1–22–11, 1995.

[7] L. Juneau, R. Hurteau, P. Freedman, and G. Chevrette. Using laser range data to model tunnel curvature for the automatic guidance of a mining vehicle. In *Proc. IEEE Conf. on Control Applications*, pages 643–648, 1993.

[8] F. Labrosse, J.-Y. Hervé, and P. Cohen. GNOMine: An application of the generic GNOME model to the representation of mines. Technical Report GRPR-RT-9611, Groupe de Recherche en Perception et Robotique, École Polytechnique, Montréal, QC, Canada, Oct. 1996.

[9] F. Labrosse, J.-Y. Hervé, and P. Cohen. GNOME: a generic object model. Technical Report GRPR-RT-9608, Groupe de Recherche en Perception et Robotique, École Polytechnique, Montréal, QC, Canada, Feb. 1996.

[10] S. E. Masry, Y. Lee, M. Kavouras, and E. C. Reeler. Digital mapping for mining applications. In *Proc. 5th Int. (FIG) Symp. Deformation Measurement and 5th Canadian Symp. on Mining Surveying and Rock Deformation Measurements*, pages 330–338, Fredericton, NB, Canada, June 1988.

[11] B. Nader, C. S. Valadao, and A. F. Ferreira. Computer application in a mining project. *Mining Mag.*, pages 297–299, May 1994.

[12] L. D. Pareja and C. W. Pelley. Solid modelling techniques for underground hard-rock mine design and planning. In *Proc. Canadian Conf. on Comp. Appl. in the Mineral Industry*, pages 149–158, 1995.

[13] H.-O. Peitgen and D. Saupe, editors. *The Science of Fractal Images*. Springer-Verlag, 1988.

[14] A. Wheeler. Developments in computerised underground mine planning. *Mining Mag.*, pages 279–280, May 1993.

[15] W. R. Williams. *Mine Mapping and Layout*. Prentice-Hall, 1983.